Article

Cell Reports

Integrative Analysis of PRKAG2 Cardiomyopathy iPS and Microtissue Models Identifies AMPK as a Regulator of Metabolism, Survival, and Fibrosis

Graphical Abstract

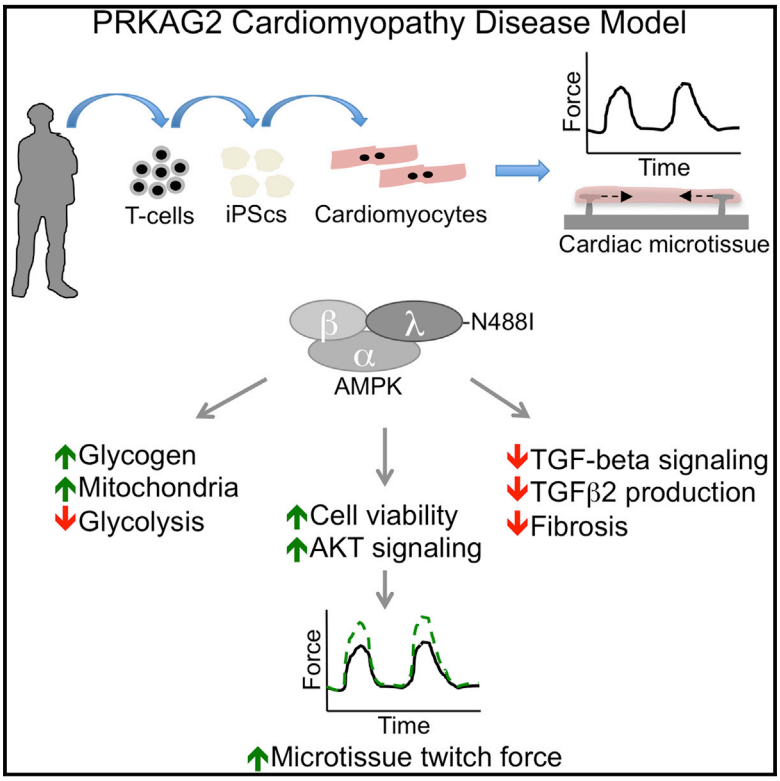

Highlights

- PRKAG2 cardiomyopathy mutations activate AMPK in human iPS models
- AMPK transcriptionally regulates glucose handling and mitochondrial biogenesis
- AMPK enhances cardiac microtissue forces by increased myocyte survival
- AMPK inhibits TGF-beta 2 production and fibrosis in vivo

Authors

J. Travis Hinson, Anant Chopra, Andre Lowe, ..., Christopher S. Chen, Jonathan G. Seidman, Christine E. Seidman

Correspondence

travis.hinson@jax.org (J.T.H.), cseidman@genetics.med.harvard.edu (C.E.S.)

In Brief

Hinson et al. now use human iPS models of PRKAG2 cardiomyopathy combined with engineered cardiac microtissues to reveal key links between metabolic sensing by AMPK and myocyte survival, metabolism, and TGF-beta signaling.

Hinson et al., 2016, Cell Reports *17*, 3292–3304
December 20, 2016
http://dx.doi.org/10.1016/j.celrep.2016.11.066

CellPress

OPEN ACCESS
CellPress

Cell Reports
Article

Integrative Analysis of PRKAG2 Cardiomyopathy iPS and Microtissue Models Identifies AMPK as a Regulator of Metabolism, Survival, and Fibrosis

J. Travis Hinson,[1,2,13,*] Anant Chopra,[3,4] Andre Lowe,[1] Calvin C. Sheng,[5] Rajat M. Gupta,[6] Rajarajan Kuppusamy,[7] John O'Sullivan,[8] Glenn Rowe,[9] Hiroko Wakimoto,[5] Joshua Gorham,[5] Michael A. Burke,[5,6] Kehan Zhang,[3,4] Kiran Musunuru,[10] Robert E. Gerszten,[8,11] Sean M. Wu,[7] Christopher S. Chen,[3,4] Jonathan G. Seidman,[5] and Christine E. Seidman[5,6,12,*]

[1]The Jackson Laboratory for Genomic Medicine, Farmington, CT 06032, USA
[2]Cardiology Center, University of Connecticut Health, Farmington, CT 06030, USA
[3]Department of Biomedical Engineering, Boston University, Boston, MA 02215, USA
[4]The Wyss Institute for Biologically Inspired Engineering at Harvard University, Boston, MA 02115, USA
[5]Department of Genetics, Harvard Medical School, Boston, MA 02115, USA
[6]Division of Cardiovascular Medicine, Brigham and Women's Hospital, Boston, MA 02115, USA
[7]Division of Cardiovascular Medicine, Cardiovascular Institute, Stanford University School of Medicine, Stanford, CA 94305, USA
[8]Division of Cardiovascular Medicine, Massachusetts General Hospital, Boston, MA 02114, USA
[9]Division of Cardiovascular Disease, University of Alabama at Birmingham, Birmingham, AL 35294, USA
[10]Penn Cardiovascular Institute, University of Pennsylvania, Philadelphia, PA 19104, USA
[11]Division of Cardiovascular Medicine, Beth Israel Deaconess Hospital, Boston, MA 02115, USA
[12]Howard Hughes Medical Institute, Chevy Chase, MD 20815, USA
[13]Lead Contact
*Correspondence: travis.hinson@jax.org (J.T.H.), cseidman@genetics.med.harvard.edu (C.E.S.)
http://dx.doi.org/10.1016/j.celrep.2016.11.066

SUMMARY

AMP-activated protein kinase (AMPK) is a metabolic enzyme that can be activated by nutrient stress or genetic mutations. Missense mutations in the regulatory subunit, PRKAG2, activate AMPK and cause left ventricular hypertrophy, glycogen accumulation, and ventricular pre-excitation. Using human iPS cell models combined with three-dimensional cardiac microtissues, we show that activating PRKAG2 mutations increase microtissue twitch force by enhancing myocyte survival. Integrating RNA sequencing with metabolomics, PRKAG2 mutations that activate AMPK remodeled global metabolism by regulating RNA transcripts to favor glycogen storage and oxidative metabolism instead of glycolysis. As in patients with PRKAG2 cardiomyopathy, iPS cell and mouse models are protected from cardiac fibrosis, and we define a crosstalk between AMPK and post-transcriptional regulation of TGFβ isoform signaling that has implications in fibrotic forms of cardiomyopathy. Our results establish critical connections among metabolic sensing, myocyte survival, and TGFβ signaling.

INTRODUCTION

PRKAG2 is one of three regulatory subunits of the AMP-activated protein kinase (AMPK) and is highly expressed in the heart (Lang et al., 2000). The activity of AMPK is determined physiologically by energy status. Changes in AMPK activity have been observed in acquired forms of cardiac remodeling such as pressure overload (Tian et al., 2001) and inherited as autosomal-dominant left ventricular hypertrophy (LVH) caused by PRKAG2 missense mutations (Gollob et al., 2001). In vitro studies indicate that PRKAG2 mutations decrease the nucleotide-dependence of AMPK catalytic activity (Scott et al., 2004), resulting in gain of function. Once activated, AMPK regulates multiple metabolic pathways including increased glucose uptake by GLUT4 translocation (Kurth-Kraczek et al., 1999) and glycolysis by phosphofructokinase-2 regulation (Marsin et al., 2000). In addition to its metabolic effects, AMPK regulates diverse energy-dependent cellular functions including protein synthesis, autophagy, cytoskeletal dynamics, and cell polarity (Hardie et al., 2012).

PRKAG2 mutations are identified in about 1% of patients with unexplained LVH (Murphy et al., 2005). PRKAG2 cardiomyopathy mimics some features of hypertrophic cardiomyopathy (HCM), a genetic disorder caused by mutations in contractile components of the sarcomere, but with notable differences. HCM, but not PRKAG2, mutations exhibit myocyte disarray and markedly increased fibrosis (Ho et al., 2010). By contrast, PRKAG2 mutations cause electrophysiologic abnormalities such as atrioventricular conduction disease and mal-development of the annulus fibrosus that predisposes to ventricular pre-excitation (Arad et al., 2002). Some features of the PRKAG2 cardiomyopathy can be explained by alterations in glucose handling (Kim et al., 2014), which leads to increased glycogen accumulation in myocytes and LVH (Arad et al., 2002). Mechanisms for the paucity of myocardial fibrosis in PRKAG2

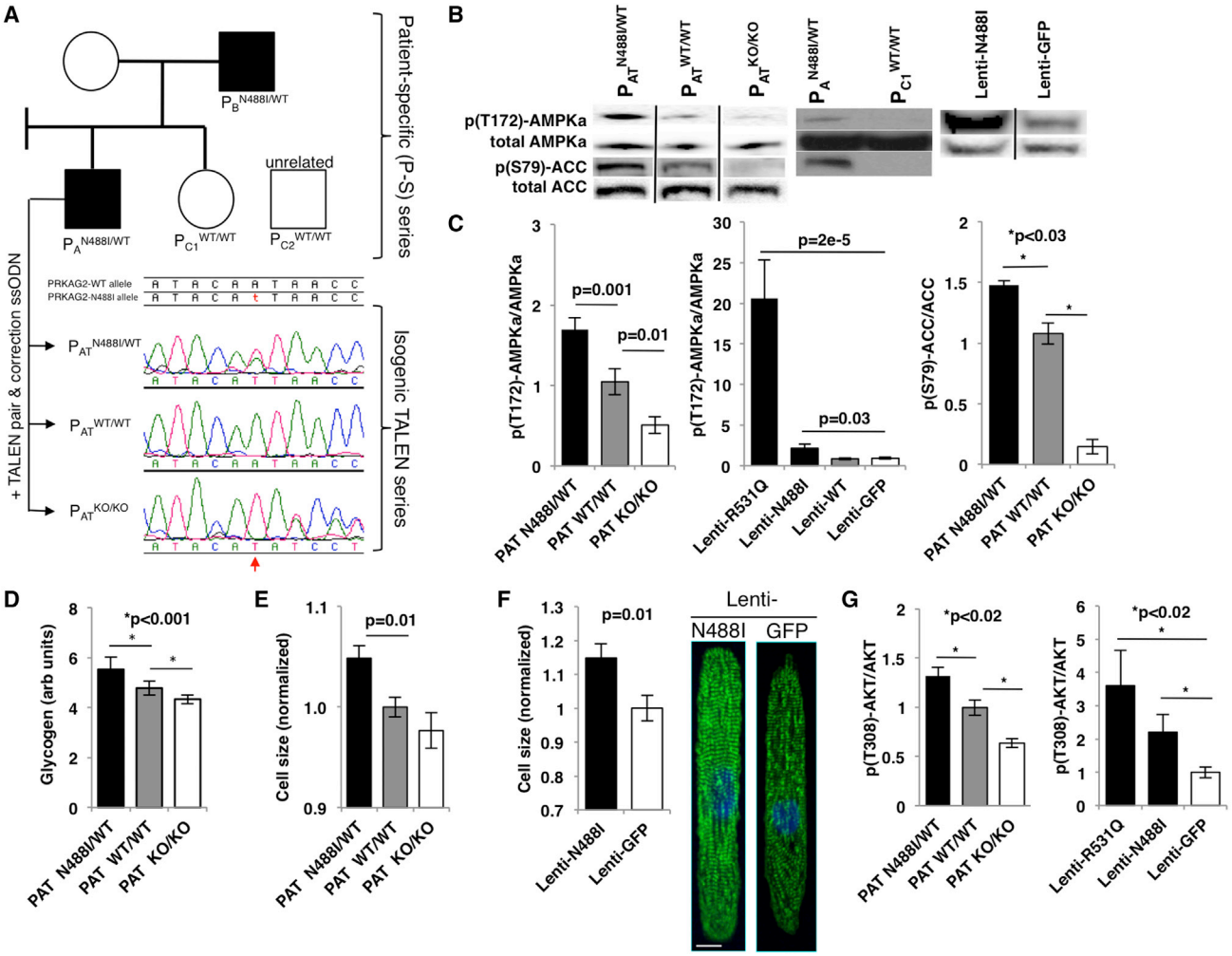

Figure 1. PRKAG2 Cardiomyopathy iPS-CMs Recapitulate Hypertrophy and Glycogen Accumulation Due to AMPK Activation

(A) IPSCs were engineered from two affected individuals ($P_A^{N488I/WT}$ and $P_B^{N488I/WT}$) and a related ($P_{C1}^{WT/WT}$) and unrelated control ($P_{C2}^{WT/WT}$) (circle = female; square = male; shaded = PRKAG2 cardiomyopathy; unshaded = normal heart). $P_A^{N488I/WT}$ iPSCs were genome-edited with TALENs and a wild-type PRKAG2 oligonucleotide to create an isogenic series at the N488I locus ($P_{AT}^{N488I/WT}$, $P_{AT}^{WT/WT}$, and $P_{AT}^{KO/KO}$). Sanger tracings of PRKAG2 amplicons derived from the isogenic TALEN series (red arrow = A/T substitution) are shown.

(B and C) Representative immunoblots (B) probed with anti-p(T172)-AMPKα subunit, p(S79)-ACC, and total AMPKα and ACC and quantified by densitometric analysis ($n \geq 3$) (C).

(D) Quantification of intracellular glycogen in iPS-CMs ($n \geq 3$).

(E and F) IPS-CM size measured by normalized forward scatter (FSC) by flow cytometry ($n \geq 15$ differentiations) (E) and by pixel area on fibronectin lines ($n \geq 20$ myocytes) (F; left panel); representative myocytes stained with anti-cardiac actinin A (green) and DAPI (blue; the scale bar represents 10 microns) (F; right panel).

(G) Quantification of anti-p(T308)-AKT by normalized densitometry ($n \geq 3$ lanes each) of immunoblots from lysates derived from iPS-CMs. The significance was assessed by Student's t test (C–G) and the error bars are mean ± SEM (C–G).

cardiomyopathy prior to end-stage disease (Pöyhönen et al., 2015) remain an enigma.

We developed two human in vitro models of PRKAG2 cardiomyopathy to study AMPK function using myocytes (iPS-CMs) differentiated from induced pluripotent stem cells (iPSCs) from patients and by TALEN genome engineering. We analyzed function in myocytes and cardiac microtissue (CMT) assays that better recapitulate cardiac architecture and myocyte maturation (Boudou et al., 2012; Hinson et al., 2015). We combined these in vitro analyses with mouse models to further probe the mechanisms that distinguish PRKAG2 from HCM mutations.

RESULTS

PRKAG2 Mutations Increase AMPK Activity, Glycogen Accumulation, and AKT Signaling Resulting in iPS-CM Hypertrophy

A patient-specific (P-S) iPSC model was engineered from members of a large family (Arad et al., 2002) with a heterozygous, missense mutation in PRKAG2 substituting asparagine for isoleucine at residue 488 (N488I). To create P-S iPSCs (Figure 1A), we reprogrammed T cells from two affected family members ($P_A^{N488I/WT}$ and $P_B^{N488I/WT}$), one unaffected relative

($P_{C1}^{WT/WT}$) and one unaffected and unrelated control ($P_{C2}^{WT/WT}$). In parallel, we engineered a series of scarless, isogenic iPSC lines derived from $P_A^{N488I/WT}$ by electroporation of TALE-nucleases (TALENs) (Ding et al., 2013) with wild-type single-stranded donor oligonucleotide that target sequences flanking the N488I mutation (Figures 1A, S1A, and S1B). The TALEN isogenic series included an unmodified N488I mutation ($P_{AT}^{N488I/WT}$), wild-type-corrected PRKAG2 ($P_{AT}^{WT/WT}$), and homozygous null alleles in PRKAG2 ($P_{AT}^{KO/KO}$).

IPSCs were then differentiated to iPS-CMs and purified by metabolic selection. Since prior publications reported conflicting effects of N488I on AMPK activity in vivo (Arad et al., 2003; Sidhu et al., 2005), we initially measured phosphorylation of AMPKα at threonine 172. Both $P_A^{N488I/WT}$ and $P_{AT}^{N488I/WT}$ iPS-CMs had similarly increased basal AMPKα phosphorylation compared to controls, while $P_{AT}^{KO/KO}$ has the lowest AMPKα phosphorylation (Figures 1B and 1C). We deduced that the TALEN isogenic series is a model of gain and loss of function in AMPK activity. We extended these studies to characterize a second AMPK missense mutation, R531Q, which causes profound neonatal PRKAG2 cardiomyopathy (Burwinkel et al., 2005). Using a lentiviral system, we expressed N488I and R531Q in iPS-CMs. While lenti-N488I increased AMPKα phosphorylation 2× compared to lenti-wild-type (WT) and GFP controls, lenti-R531Q increased AMPKα phosphorylation by over 20× (Figure 1C, middle panel). N488I also increased acetyl-CoA carboxylase (ACC) phosphorylation at the AMPK target site serine 79 (Figure 1C, right panel). These results confirm that N488I and R531Q mutations that cause PRKAG2 cardiomyopathy increase AMPK activity in proportion to the degree of cardiomyopathy severity.

Next, we used the TALEN isogenic series to model the consequences of gain and loss of function in AMPK activity. Glycogen content in $P_{AT}^{N488I/WT}$ iPS-CMs was 17% higher than in $P_{AT}^{WT/WT}$ iPS-CMs, while the glycogen content in $P_{AT}^{KO/KO}$ iPS-CMs was the lowest (Figure 1D). We analyzed iPS-CM size by flow cytometry and after patterning iPS-CMs onto fibronectin lines to align sarcomeres to more closely resemble in vivo sarcomere structure (Figures 1E, 1F, and S1J). By either method, N488I iPS-CMs were larger. Mutant iPS-CMs also had increased insulin signaling, a recognized hypertrophic signal, as supported by increased AKT phosphorylation at threonine 308 (Figure 1G). These data confirm that LVH associated with PRKAG2 cardiomyopathy correlates with both glycogen accumulation and myocyte hypertrophy that is associated with AKT phosphorylation.

AMPK Increases Microtissue Twitch Force by Enhancing Myocyte Survival

Unlike mutations in beta-myosin heavy chain that cause HCM by altering properties of contractile components (Debold et al., 2007), whether AMPK regulates cardiac force production remains unknown. To address this, we measured twitch force in CMTs that are composed of iPS-CMs (Movies S1 and S2). $P_{AT}^{N488I/WT}$ CMTs generated 6.16 μN of twitch force compared to 2.81 μN by $P_{AT}^{WT/WT}$ CMTs ($p = 1.5 \times 10^{-6}$; Figure 2A), an increase that remained after normalization for CMT width (Figure 2B). As twitch force in CMTs is dependent on cell composition and maturity, we expressed N488I or GFP by lentiviral transduction into iPS-CMs with identical iPS-CM content and made CMTs. Lenti-N488I similarly increased twitch force by 98% ($p = 4 \times 10^{-5}$; Figure 2C). Next, iPS-CMTs were stained with the sarcomeric isoform of actinin A and nuclear stain DAPI (Figure 2D) to identify structural changes that may explain increased CMT twitch force. Analysis of stained $P_{AT}^{N488I//WT}$ CMTs identified a 51% increase (Figure 2E; $p = 5.7 \times 10^{-6}$) in iPS-CM number despite controlling for iPS-CM seeding density. Since single cell traction force assays were not different in iPS-CMs with N488I (Figure S2A), and expression of maturity and chamber-specific transcript markers were also not regulated by N488I (Figures S2B–S2E), we conclude that $P_{AT}^{N488I/WT}$ CMTs have increased iPS-CM number per CMT as the major mechanism for increased CMT twitch force.

To consider whether the increase in iPS-CM number was due to increased iPS-CM survival or proliferation, we stained live CMTs with propidium iodide (PI), which penetrates and binds DNA only in non-viable cells. As $P_{AT}^{N488I/WT}$ CMTs had 37% fewer PI-positive nuclei ($p = 6 \times 10^{-4}$; Figures 2F and 2G), we deduced that N488I increased iPS-CM survival in CMT assays, but did not alter proliferation rates since BRDU+ and cyclin B1 expression were not increased in $P_{AT}^{N488I/WT}$ iPS-CMs (Figures S2F and S2G). Consistent with increased survival, $P_{AT}^{N488I/WT}$ iPS-CMs cultured routinely in standard tissue culture were 33% more viable at baseline ($p = 0.03$; Figure 2H, left panel) and after exposure to the cardiotoxic agent doxorubicin ($p = 0.02$; Figure S2H). To determine whether the enhanced viability was due to inhibition of apoptosis, we measured caspase-3/7 cleavage in iPS-CMs. While overall cytotoxicity was decreased by 14% ($p = 0.05$; Figure 2H, middle panel) in $P_{AT}^{N488I/WT}$ iPS-CMs consistent with PI staining, cell death by apoptosis was increased by 48% ($p = 5 \times 10^{-6}$; Figure 2H, right panel). These results indicate that AMPK enhances twitch force in CMTs by inhibiting non-apoptotic cell death.

AMPK Regulates Metabolism by Transcript Regulation

Since PRKAG2 cardiomyopathy is associated with life-long AMPK changes, we speculated that transcript regulation would reflect mechanisms of the genetic disorder. We analyzed gene transcripts by RNA sequencing (RNA-seq) of iPS-CMs derived from P-S and TALEN isogenic cohorts (Figure 3A; Tables S3 and S4). We then performed unsupervised principle component analysis (PCA) of expression patterns to identify transcripts that separate cells within P-S and TALEN isogenic models (Figures 3B and 3C; Table S5). In both data sets, iPS-CMs with N488I were separated from controls by the first two principle components. PC 1 (PC1) included components of the cardiac sarcomere including myosin heavy chains (*MYH6* and *7*), myosin light chains (*MYL3*, *4*, and *7*) and thin filament components (*TNNT2*, *TNNC1*, and *ACTC1*). Moreover, PC1 contained genes associated with hypertrophy, such as ribosomal and translational transcripts (*RPL41*, *EEF1A1*, *RPL37A1*, and *RPL37*) and atrial-type natriuretic peptide (*NPPA*). PC 2 (PC2) contained gene transcripts involved in extracellular matrix (ECM) including collagens (*COL11A1*, *COL1A1*, *COL3A1*, *COL1A2*, and *COL6A3*) and ECM regulators (*THBS2*, *LOX*, *BGN*, and *SERPINE2*). PC2 also contained gene transcripts involved in cytoskeletal dynamics

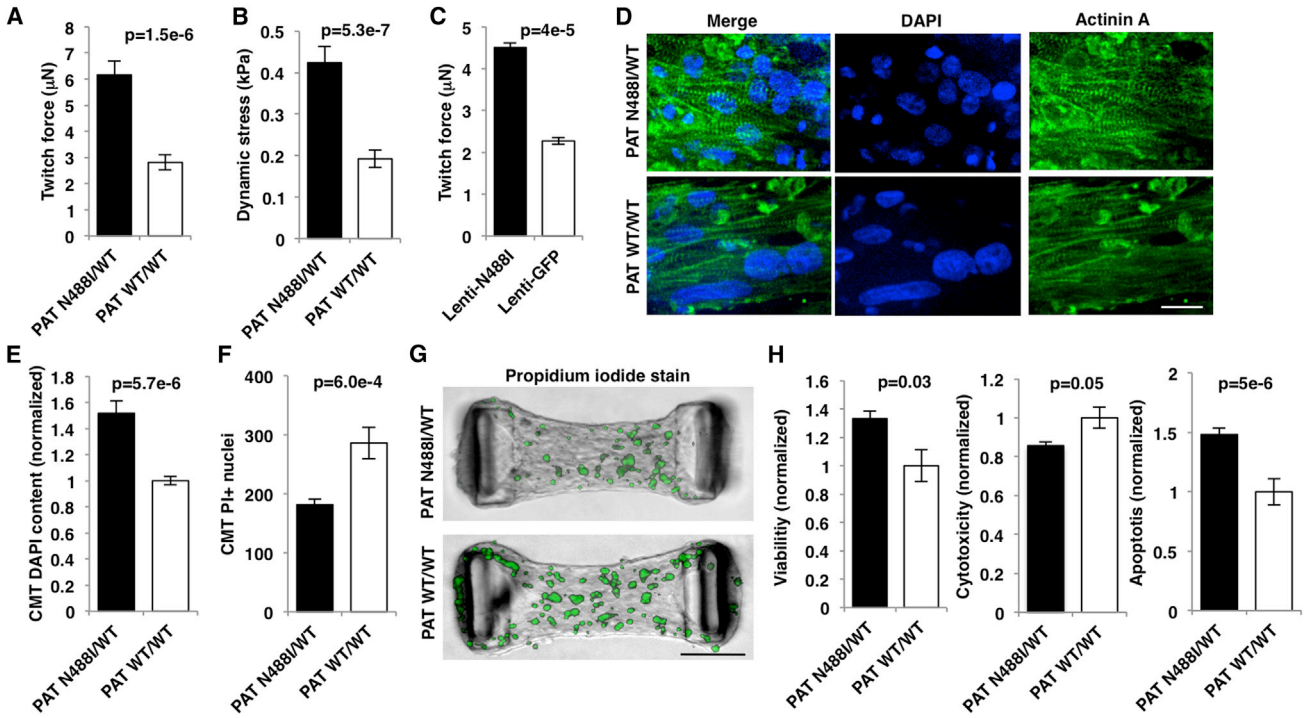

Figure 2. AMPK Increases Twitch Force by Enhancing Viability in Microtissues

(A) Twitch force (μN) measured by cantilever displacement by CMTs generated from iPS-CMs and paced at 1 Hz ($n \geq 5$ CMTs).

(B) Tissue dynamic stress measured by twitch force normalized to CMT cross-sectional area ($n \geq 5$ CMTs).

(C) Twitch force (μN) from IPS-CMs transduced with lentivirus expressing N488I or GFP ($n \geq 5$ CMTs).

(D) Representative CMTs fixed and immunostained with anti-cardiac actinin A (green) to highlight sarcomeres and DAPI (blue) to identify nuclei (the scale bar represents 20 microns).

(E) Normalized nuclear content in CMTs by DAPI staining ($n \geq 10$ CMTs).

(F) Non-viable cells in live CMTs labeled with PI ($n \geq 10$ CMTs).

(G) Representative CMTs stained with PI (green) to identify dead cells (the scale bar represents 100 microns).

(H) IPS-CMs were cultured on tissue culture plates and analyzed for viability (left), cytotoxicity (middle), and apoptosis (right panel) ($n \geq 6$ replicates). The significance was assessed by Student's t test (A–C, E, F, and H) and the error bars are mean ± SEM (A–C, E, F, and H).

(*ACTG2* and *MYLK*). Analysis of combined PC1 and PC2 transcripts by hierarchical clustering and illustrated in a heatmap (Figures 3D and 3E) confirmed shared gene expression patterns between iPS-CMs with PRKAG2-N488I.

We proceeded to analyze differentially regulated gene transcripts from TALEN isogenic and P-S iPS-CM cohorts (Figure 4A). We identified 623 differentially regulated transcripts in the P-S cohort and 1,660 in the TALEN isogenic cohort (Tables S3 and S4). Differentially regulated transcripts were then analyzed by pathway analysis using Ingenuity Pathway Analysis (IPA) and ranked by *Z* score of enrichment. Like PCA, analysis of pathways enriched in both iPS-CM cohorts identified highly correlated (r = 0.69) pathways increased in both N488I iPS-CM models (Figure 4B). Key metabolic factors were enriched in iPS-CMs with PRKAG2-N488I including regulators of mitochondrial biogenesis and oxidative metabolism, such as PGC-1α, PPARγ, PPARα, HNF-4α, and estrogen-related receptor α. Chemical agonists of these pathways were also identified, including guanidinopropionic acid (Reznick et al., 2007), rosiglitazone (Lehmann et al., 1995), and mono-(2-ethylhexyl) phthalate (Lovekamp-Swan et al., 2003). The N488I mutation increased RNA transcripts associated with increased microRNA activity that regulated myocyte differentiation (miR-124) (Cai et al., 2012) and pathologic cardiac hypertrophy (miR-1) (Ikeda et al., 2009), as well as transcripts downstream of signaling by the insulin receptor family (INSR and IGF1R).

Because of increased glycogen storage, we analyzed glucose transporters and the rate-limiting enzymes that regulate glycogen content. Transcript data indicated that N488I mutation favored glycogen accumulation by coordinated regulation of key glucose handling transcripts. $P_{AT}^{N488I/WT}$ iPS-CMs have increased insulin-dependent GLUT4 (*SLC2A4*; Figure 4C) transcripts that are responsible for the majority of glucose transport in myocytes (Kraegen et al., 1993), but reduced levels of GLUT1 (*SLC2A1*). In parallel, transcripts encoding glycogen synthase (*GYS1*) were increased in $P_{AT}^{N488I/WT}$ iPS-CMs, while glycogen phosphorylase, the rate–limiting glycogen degradation enzyme, shifted from the more AMP-sensitive brain isoform (*PYGB*) to the less AMP-sensitive muscle isoform (*PYGM*) (Lehmann et al., 1995) (Figure 4D).

To explore how AMPK regulates glycolysis and fatty acid oxidation, we analyzed transcripts in these pathways. $P_{AT}^{N488I/WT}$

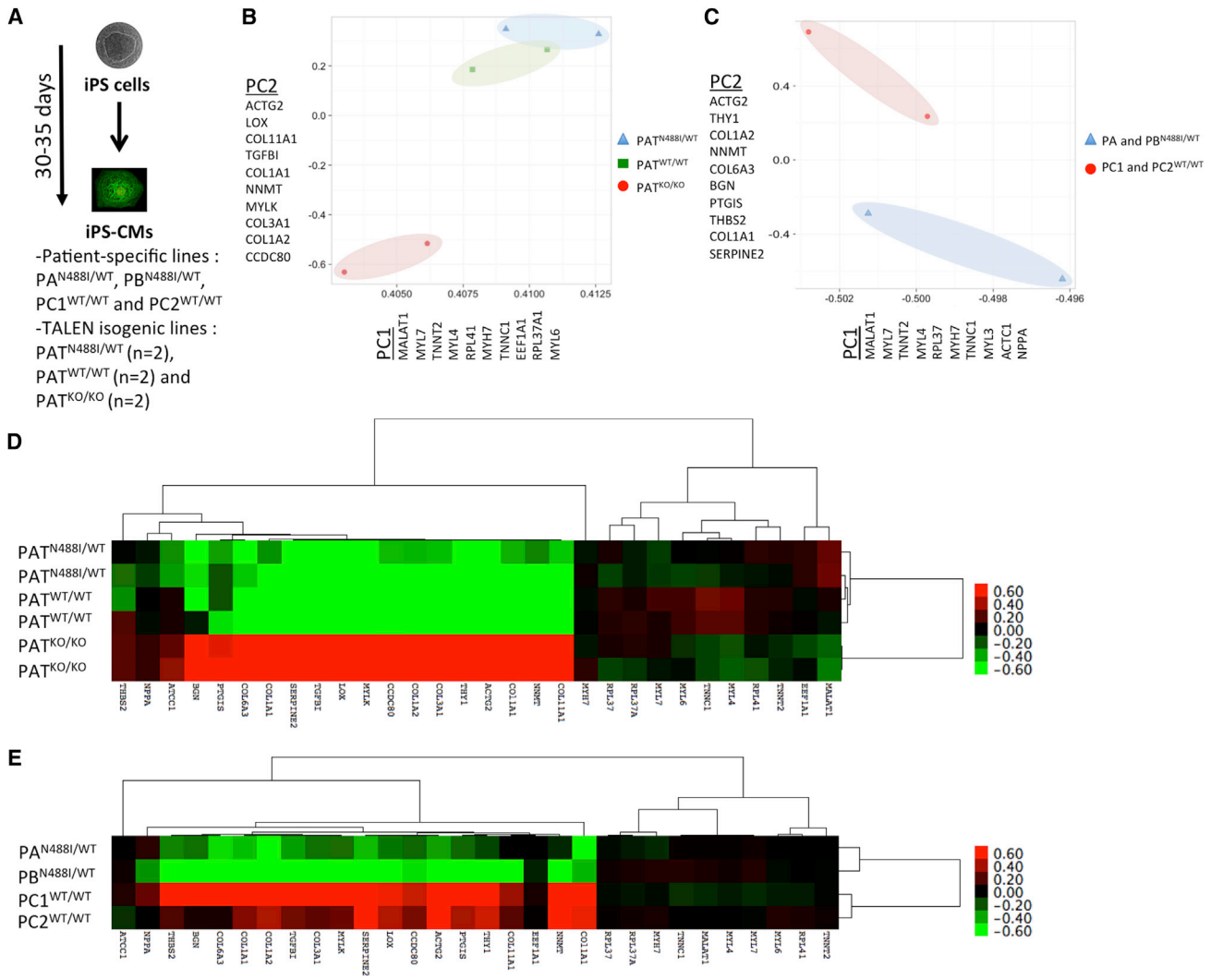

Figure 3. Gene Expression Analysis by RNA-Seq of TALEN and P-S iPS-CM Models

(A) Experimental design of RNA sequencing for purified P-S and TALEN isogenic iPS-CMs (pooled triplicates for P-S and duplicates of pooled triplicates for TALEN isogenic).

(B–E) Unsupervised principle components analysis (PCA) of all TALEN isogenic (B) and P-S (C) iPS-CM gene transcripts separates cell populations by genotype by PC1 and PC2. The gene components of PC1 and PC2 are identified by official gene symbol. A heatmap displays 30 gene transcripts from all PC1 and PC2 components for TALEN isogenic (n = 6 pooled triplicates) (D) and P-S iPS-CMs (n = 4 pooled triplicates) (E). The gene transcripts and iPS-CMs were organized by hierarchical clustering.

iPS-CMs exhibited an isoform switch in phosphofructokinase-1 (*PFK-1*), the rate-limiting step in glycolysis, to the less active muscle isoform from the liver isoform (Figure 4E, left panel) and favored expression of PFK-2/FBPase *PFKFB2* instead of *PFKFB3*. These changes implied that glycolysis would be less active in $P_{AT}^{N488I/WT}$ iPS-CMs (Figure 4E, right panel). Both *CD36* and *FABP3*, genes that regulate fatty acid uptake into myocytes, were increased in $P_{AT}^{N488I/WT}$ iPS-CMs (Figure 4F), a finding that is consistent with increased transcripts of regulators of mitochondrial biogenesis and oxidative phosphorylation, such as PGC1-1α itself (Figure 4G). Both mitochondrial transcripts encoded by nuclear DNA and in this organelle were also increased (Figures 4H and 4I).

To determine the functional relevance of transcript changes, we measured steady-state levels of intracellular metabolites by liquid chromatography-tandem mass spectrometry (LC-MS/MS), mitochondrial content and respiration, and glucose uptake and lactate production in conditioned media from TALEN isogenic iPS-CMs. We focused on pathways involved in glucose handling and oxidative metabolism and identified metabolites that correlated with AMPK activity, as determined by the level of p(T172)-AMPKα (Figure 1C). Among 224 metabolites detected (Figure 5A; Table S6), 70 were significantly increased ($r > 0.67$) and 78 were significantly decreased ($r < -0.67$) in $P_{AT}^{N488I/WT}$ iPS-CMs. We analyzed metabolites associated with glucose handling first. Of four measured metabolites associated with

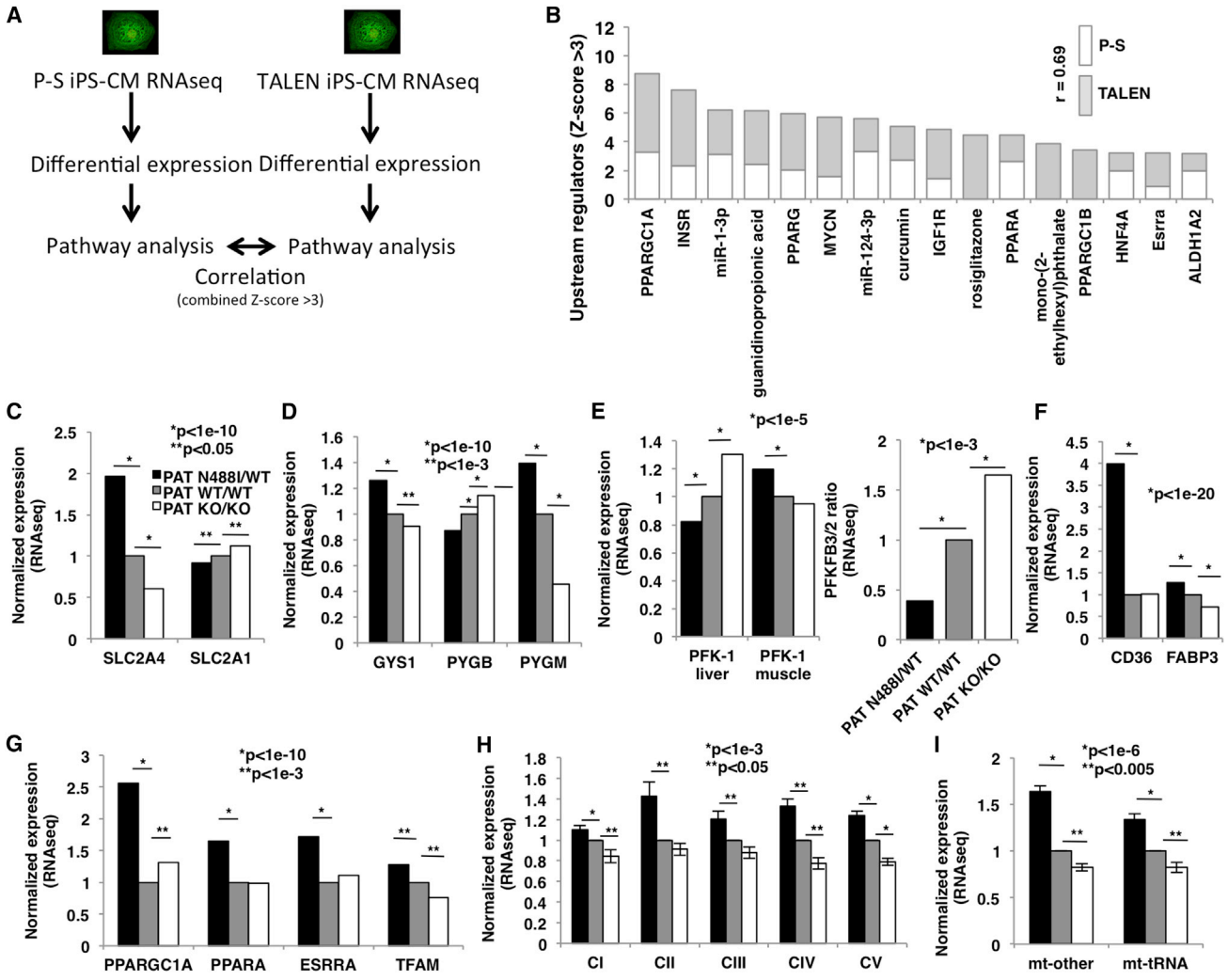

Figure 4. Pathway Analysis of RNA-Seq Transcripts Identifies Metabolic and Signaling Pathways that Regulate Glucose Handling and Oxidative Metabolism in iPS-CMs with PRKAG2-N488I

(A) Experimental overview to identify transcript pathways regulated by N488I in P-S and TALEN cohorts.

(B) Transcript pathways increased (*Z* score > 3) by N488I (P-S, no shade and TALEN isogenic, gray) associate with metabolic and growth factor signaling and are positively correlated (r = 0.69). The transcript networks include PGC-1α/β (*PPARGC1A* and *PPARGC1B*), insulin receptor (*INSR*), PPARα/γ (*PPARA* and *PPARG*), *IGF1R*, hepatocyte nuclear factor 4α (*HNF4A*), and estrogen receptor related α (*ESRRA*). The pathways regulated by *microRNAs-1* and *-124* and activators of mitochondrial biogenesis like guanidinopropionic acid, circumin, rosiglitazone, and mono-(2-ethylhexyl) phthalate are shown.

(C–F) Transcripts of glucose transporters GLUT1 (*SLC2A1*) and the insulin-sensitive GLUT4 (*SLC2A4*) (C), glycogen synthase-1 (*GYS1*) (D), isoforms of glycogen phosphorylase (PYGM [muscle] and PYGB [brain]) (D), glycolytic enzymes *PFK-1* and the bifunctional glycolysis regulator 6-phosphofructo-2-kinase/fructose 2,6-bisphosphatases *PFKFB2* and *PFKFB3* (E), and fatty acid transporters *CD36* and *FABP3* (F).

(G–I) Regulators of mitochondrial biogenesis PGC-1α, PPARα, estrogen-related receptor α, and mitochondrial transcription factor A (*TFAM*) (G). The transcripts of nuclear-encoded (merged) (H) and mitochondrial DNA-encoded (merged) genes (I) that are components of respiratory chain complexes I–V (CI–V), tRNAs (mt-tRNAs), and all other genes (mt-other) encoded by the mitochondrial DNA are shown. The data are normalized fragments per kilobase of transcript per million (FPKM) (C–I) and means ± SEM (H and I). The significance was assessed by *Z* score of enrichment (B), Bayesian p values (C–G), or Student's t test (H and I).

glycolysis with significant differences ($p < 0.05$), only glucose-6 phosphate was increased (r = 1.00) in $P_{AT}^{N488I/WT}$ iPS-CMs. By contrast, the downstream glycolytic metabolites fructose-6-phosphate (r = −0.74), 1,3-bisphosphoglycerate (r = −0.83) and 3-phosphoglycerate (r = −0.72) were significantly decreased in $P_{AT}^{N488I/WT}$ iPS-CMs (Figure 5B). Consistent with this mismatch between glucose uptake and glycolysis, the glycogen precursor glucose-1-phosphate was similarly increased (r = 0.94). To determine whether these steady-state levels reflected changes in the kinetics of glucose handling, we measured glucose uptake in conditioned media from $P_{AT}^{N488I/WT}$ iPS-CMs compared to controls. Glucose uptake was increased by 8.3% ($p = 0.008$; Figure 5C, left panel) in parallel to glucose-6-phosphate, and lactate production was decreased by 8.3% ($p = 3 \times 10^{7}$; Figure 5C, right panel) in parallel to reduction in three downstream glycolytic intermediates. Activation of AMPK by A769662

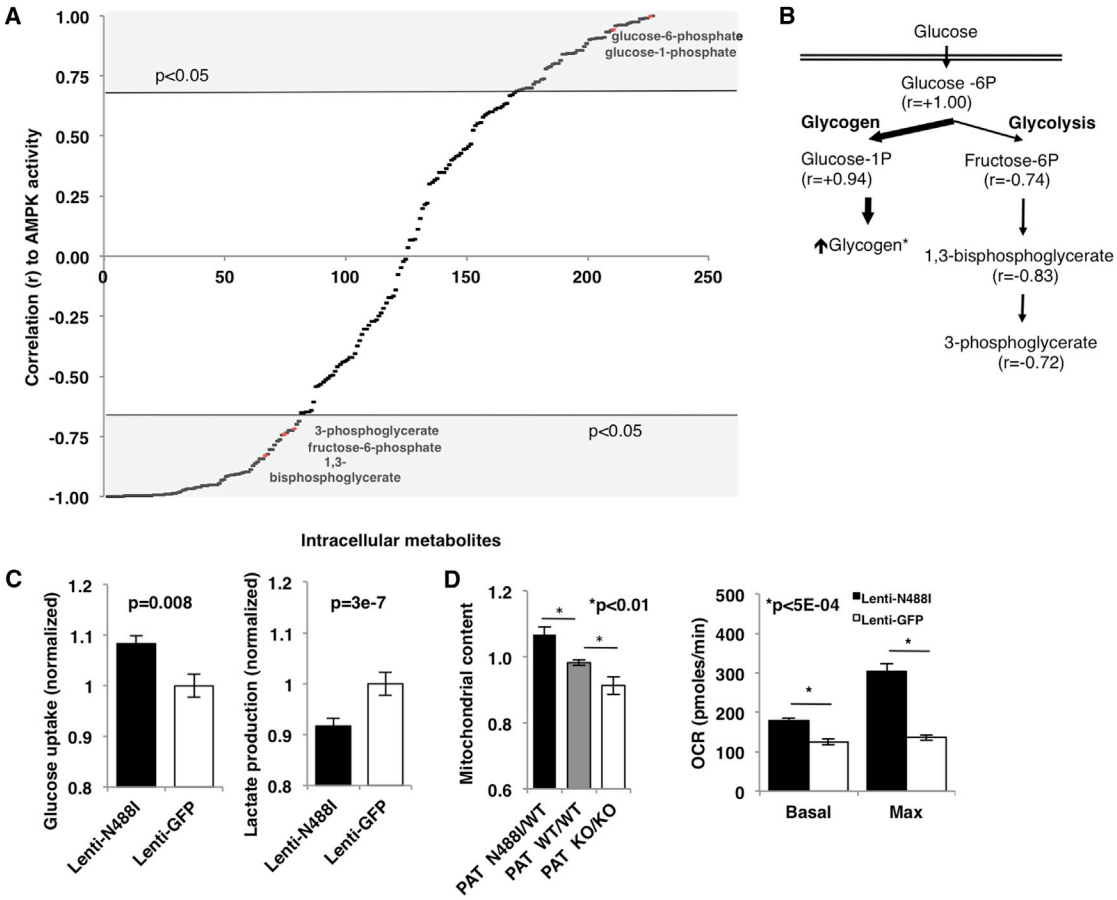

Figure 5. Metabolic Assays by LC-MS/MS, Glucose Handling, and Mitochondrial Function

(A) 224 intracellular metabolites quantified by LC-MS/MS at steady state in iPS-CMs (n = 3) and correlated (r) with AMPK activity. The metabolites shaded in gray satisfy $p < 0.05$.

(B) Schematic showing metabolites involved in glucose handling that are significantly correlated with AMPK activity.

(C) Normalized glucose uptake and lactate production by iPS-CMs (n > 3).

(D) Normalized mitochondrial content measured by FACS analysis of MitoTracker-stained iPS-CMs, and mitochondrial function measured by basal and maximum oxygen consumption rate (pmoles/min). The data are means ± SEM (C and D). The significance was assessed by Pearson correlation (A) or Student's t test (C and D).

similarly regulated glucose and lactate metabolism in iPS-CMs (Figure S3B).

Metabolic intermediates associated with fatty acid oxidation identified by LC-MS/MS were increased, including carnitine (r = 0.91), C2-, C5-, and C8-long chain acylcarnitines (r = 0.99, 0.69, and 0.70, respectively) and long chain acyl-CoA (r = 0.77). Based on the increased transcripts encoding regulators of mitochondrial biogenesis (e.g., PGC-1α and PPARα), we suggest that increased mitochondrial content and function may account for increased steady-state levels of fatty acid intermediates. Indeed, both mitochondrial content and oxygen consumption were increased in $P_{AT}^{N488I/WT}$ iPS-CMs compared to isogenic controls (Figures 5D and S3A).

AMPK Activation Inhibits TGFβ Signaling by Inhibition of TGFβ-2 Production In Vitro

RNA-seq data revealed changes in gene expression that predicted inhibition of distinct signaling networks (Figure 6A). Among these, we noted that N488I mutations reduced expression of transcript targets of TGFβ signaling and other pathways implicated in cardiac fibrosis, including rictor (RICTOR) (Li et al., 2015), thrombin (F2) (Carney et al., 1992), angiotensinogen (AGT) (Rupérez et al., 2003), endothelin-1 (EDN1) (Widyantoro et al., 2010), and the known cardiotoxic agent doxorubicin. Also, pathway regulators with functions downstream of non-canonical TGFβ signaling were predicted to be inhibited, such as MAP kinase kinase kinase kinase 4 (MAP4K4) and MAP kinase signal-integrating kinase 1 (MKNK1). In addition, specific TGFβ transcriptional targets including genes that regulate collagen crosslinking (LOXL1 and LOXL2), growth factor (CTGF), cytoskeleton (ACTN1, ACTA2, and FLNA), and signaling (LTBP2 and SMAD6) were reduced in $P_{AT}^{N488I/WT}$ iPS-CMs (Figure 6B).

As reduced activation of TGFβ pathways could account for the unusual lack of fibrosis in PRKAG2 cardiomyopathy and the loss of integrity in the annulus fibrosis, we probed canonical TGFβ

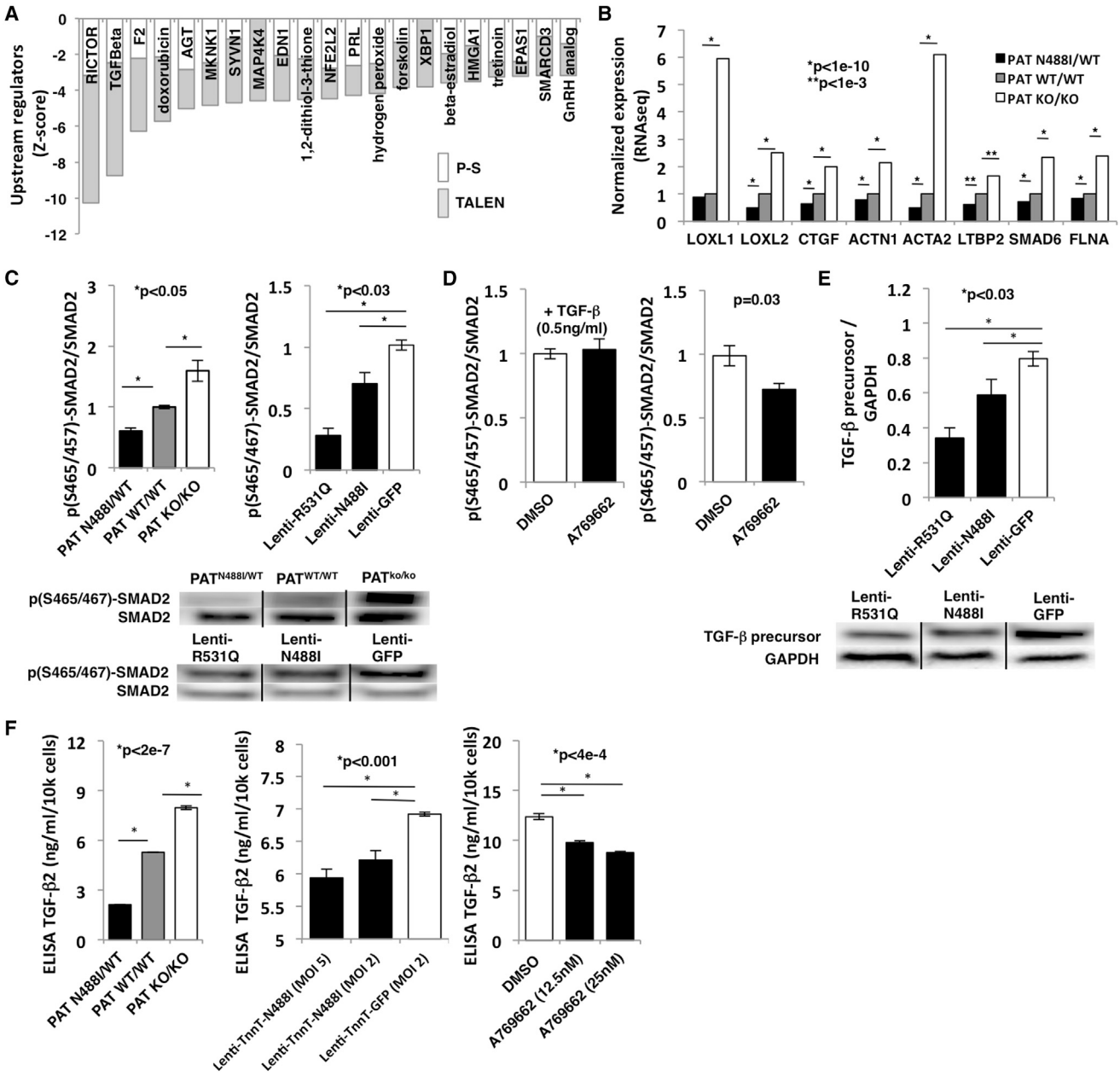

Figure 6. AMPK Inhibits Transcripts Associated with Cardiac Fibrosis In Vitro

(A) Transcript pathways depleted (*Z* score < −3) in PRKAG2-N488I iPS-CMs (P-S, no shade and TALEN isogenic, gray) include RICTOR, transforming growth factor-beta (TGFβ), thrombin (F2), doxorubicin, angiotensinogen (AGT), MAP kinase interacting kinase 1 (MKNK1) and EDN1.

(B) Transcripts of TGFβ-regulated genes: lysyl oxidase-1 and -2 (*LOXL1* and *LOXL2*), connective tissue growth factor (*CTGF*), smooth muscle alpha actinin (*ACTN1*), smooth muscle actin (*ACTA2*), latent TGFβ binding protein-2 (*LTBP2*), *SMAD6*, and filamin A (*FLNA*).

(C) Left: Immunoblots probed with anti-p(S465/457)-SMAD2 and total SMAD2 and quantified by densitometry (n > 3 per genotype) with (bottom panel) representative blots.

(D) Immunoblots analyzed from IPS-CMs pre-treated with AMPK agonist A769662 and (left panel) stimulated with 0.5 ng/mL exogenous TGFβ for 30 min or (right panel) no stimulation (n > 3 per treatment).

(E) Lysates of iPS-CMs transduced with lentivirus and probed with anti-TGFβ precursor or glyceraldehyde-3-phosphate dehydrogenase, GAPDH (n > 3 per genotype), with (bottom panel) representative blots.

(F) ELISA for TGF-β2 from conditioned media of iPS-CMs transduced with N488I expressed by troponin T promoter (MOI 2 and MOI 5) and by A769662 (12.5 and 25 nM) (n > 3 per condition). The data are normalized FPKM (B) and means ± SEM (C–F). The significance was assessed by Bayesian p value (B) or Student's t test (C–F).

signaling pathways by measuring SMAD2 phosphorylation at serine 465/457 in iPS-CMs. SMAD2 phosphorylation was inhibited in proportion to AMPK activation in both the TALEN isogenic iPS-CMs and with lenti-N488I and -R531Q to control for maturation and purity (Figure 6C). As decreased SMAD2 phosphorylation could reflect mechanisms upstream or downstream of the TGFβ receptor, we remeasured SMAD2 phosphorylation after pre-treatment with the AMPK agonist A769662 in iPS-CMs treated with or without exogenous TGFβ. Only A769662 pre-treatment without exogenous TGFβ reduced SMAD2 phosphorylation by 28% ($p = 0.03$; Figure 6D, right image), which suggested a mechanism upstream of the receptor. Furthermore, TGFβ precursor protein was reduced in iPS-CMs expressing either the N488I or R531Q mutation ($p < 0.03$; Figure 6E).

We next determined the TGFβ isoform that was regulated by AMPK by ELISA assays of conditioned culture media. $P_{AT}^{N488I/WT}$ iPS-CMs and iPS-CMs with myocyte-specific lentiviral transduction of N488I or treated with A769662 dose-dependently reduced levels of TGFβ-2 (Figure 6F), but not TGFβ-1 (Figure S4A). By contrast, we did not observe a significant relationship between AMPK activity and *TGFβ1* or *TGFβ2* transcript levels (Figure S4B). TGFβ-3 was not expressed highly in iPS-CMs (Figure S4B). In summary, PRKAG2 mutations or A769662 that activate AMPK inhibit the production of TGFβ precursor protein and leads to reduced TGFβ-2 produced in iPS-CMs by post-transcriptional regulation.

AMPK Activation Inhibits TGFβ-Regulated Transcripts In Vivo

We hypothesized that AMPK activation might provide a therapeutic strategy to inhibit pathological forms of cardiac remodeling that are associated with fibrosis, such as in HCM where TGFβ signaling is increased (Teekakirikul et al., 2010). We initially analyzed transcripts associated with fibrosis in RNA-seq data from pre-hypertrophic mice with PRKAG2 cardiomyopathy (Arad et al., 2003) with RNA-seq from wild-type and pre-hypertrophic HCM mice ($MHC^{R403Q/+}$) (Geisterfer-Lowrance et al., 1996). Similar to iPS-CM models, N488I mice had reduced expression of TGFβ targets that are associated with fibrosis including extracellular matrix components and regulators (Figure 7A), which is in contrast to HCM mice. Human histopathology (Figure 7B) was consistent with these data. LV sections stained with Mason trichrome showed little fibrosis in a patient with PRKAG2 (N488I) cardiomyopathy compared to HCM ($MYBPC3^{+/-}$). Therefore, while lifelong, constitutive AMPK activation leads to the PRKAG2 cardiomyopathy, a method to provide a tunable AMPK activation could achieve reduction in gene transcripts involved in fibrosis that are regulated by TGFβ in vivo.

Next, we tested whether the AMPK agonist A769962 could prevent the development of hypertrophy and fibrosis in HCM mice. We treated 6-week-old pre-hypertrophic HCM mice with A769662, using a once instead of twice daily dose that did not change weight, blood pressure, or glucose (Cool et al., 2006). A769662-treated HCM mice developed less hypertrophy (1.32 mm versus 1.55 mm, $p = 0.04$; Figure 7C) and tissue fibrosis (5.02% compared to 6.85%, $p = 0.002$; Figure 7D) compared to carrier-treated HCM mice. LV transcriptional analyses of A769662-treated HCM mice identified 2,768 differentially expressed genes compared to controls (Table S7). Comparison of pathway analyses (IPA) of differentially expressed genes from the in vitro TALEN isogenic iPS-CM cohort with in vivo A769662-treated HCM mice, were highly correlated ($r = 0.60$). The activation states of multiple pathways were common to both, including TGFβ that was the most negatively regulated pathway in vivo (Z score of −9.1; Figure 7E). Moreover, A769662-treated HCM mice had markedly reduced cardiac expression of the same TGFβ targets, including extracellular matrix components and regulators reduced in pre-hypertrophic N488I mice (Figure 7F). In addition, A769662-treatment reduced hypertrophic gene expression (*NPPA* and *NPPB*), normalized myosin isoform expression (*MYH7*/*MYH6* ratios), and increased oxidative transcripts (e.g., *PGC-1α* and *PPARα*) in HCM hearts (Figures 7G and 7H) and in control hearts (Figure S5).

DISCUSSION

AMPK coordinates metabolic sensing with a diverse group of energy-dependent cellular functions. The integration of biochemical, transcriptional, and functional data sets using human iPS-CMs, microtissues, and mouse models allowed us to deconvolute how mutations produce the phenotypes observed in PRKAG2 mutations. Our analyses of human iPS-CMs provide evidence that PRKAG2 mutations increase myocyte size in correlation with increased glycogen content and by activating AKT signaling, which is consistent with findings in PRKAG2 mouse models (Kim et al., 2014). We further demonstrate that regulation of glucose metabolism that results in glycogen accumulation by PRKAG2 mutations is due to coordinated changes in transcript abundance of key regulators of glucose handling. While other studies have defined the acute or chronic effects of AMPK activity on specific factors (Bultot et al., 2012; McGee et al., 2008), this study is the first to define the transcriptional network that drives glycogen accumulation. For example, we find increased transcripts encoding glycogen synthase, and isoform shifts in glycogen phosphorylase, phosphofructokinase, and glucose transporters that parallel changes in steady-state metabolomics and glucose handling kinetics. On the other hand, we identify mitochondrial biogenesis factors increased, such as PGC-1α and PPARα, which parallel increased mitochondrial content and respiration. This pattern of metabolic remodeling is opposite to the changes associated with heart failure (Doenst et al., 2013), which is reflected in the iPS-CMs by reduced transcripts associated with heart failure such as natriuretic peptides.

Unexpectedly, the metabolic and transcriptional changes induced by mutational activation of AMPK were associated with increased viability leading to increased twitch force in microtissues. These observations are consistent with in vivo studies that indicate increased AMPK activation can protect the heart from ischemic stress (Ofir et al., 2008). Several mechanisms could account for the improved stress response, including increased AKT signaling observed here, glycogen content that would provide a ready supply of glucose, that is the preferred energy substrate in stressed myocytes (Ofir et al., 2008), increased mitochondrial biogenesis, and activation of

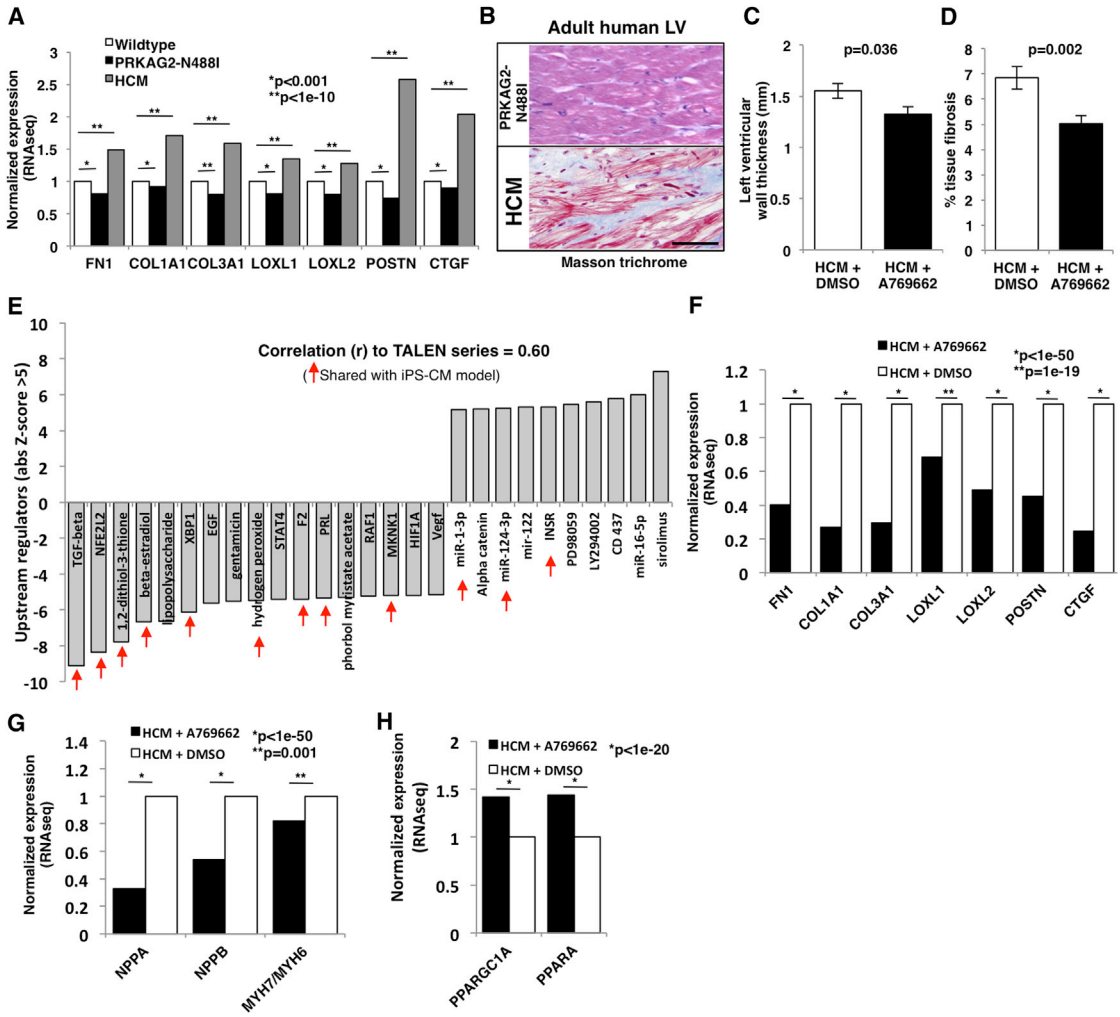

Figure 7. AMPK Prevents Cardiac Fibrosis and Pathologic Hypertrophy In Vivo

(A) Transcripts by RNA-seq of TGFβ targets from mouse left ventricular tissue with pre-hypertrophic PRKAG2 cardiomyopathy (N488I; black bars), pre-hypertrophic HCM (gray bars), and wild-type controls (white bars).

(B) Representative formalin-fixed sections stained with Masson trichrome (fibrosis = blue) in adult human LV tissue from patient $P_A^{N488I/WT}$ compared to HCM (MYBPC3 mutation). The scale bar represents 100 microns.

(C) Pre-hypertrophic HCM mice were treated with A769662, and hypertrophy was measured by LV wall thickness (n > 15 mice per condition).

(D) Tissue fibrosis (%) measured by Masson trichrome staining (n > 35 sections from >3 mice per condition).

(E) Transcript pathway analysis of transcripts from HCM mice treated with A769662 or carrier were identified and compared to transcript pathways identified from iPS-CM models (shared = red arrows).

(F–H) Transcript levels of TGFβ targets, pathological hypertrophy genes (G), and mitochondrial biogenesis factors from HCM mice treated with A769662 (H). The data are normalized FPKM (A and F–H) and mean ± SEM (C and D). The significance was assessed by Bayesian p value (A and F–H) or Student's t test (C and D).

autophagy (Baskin and Taegtmeyer, 2011). We recognize that the heightened viability and twitch force of mutant myocytes contrasts with the poor clinical courses of adult patients and mice with PRKAG2 cardiomyopathy (Murphy et al., 2005). We suggest several observations that account for these differences. First, cardiac conduction system cells that were not modeled in these studies with PRKAG2 mutations progressively develop dysfunction and contribute substantially to in vivo phenotypes. Second, late-onset cardiac deficits of PRKAG2 mutations may not be well modeled in short-term tissue culture studies. Finally, as both embryonic myocytes and immature iPS-CMs routinely metabolize glucose for energy, these cells may have multiple adaptations to accommodate excess glucose and glycogen.

Unlike most other forms of LVH including HCM, PRKAG2 cardiomyopathy is distinguished by a remarkable absence of myocardial fibrosis. Attenuated TGFβ signaling, that we identified in both iPS-CMs and mouse models of PRKAG2 cardiomyopathy, appears to account for the absence in fibrosis. While others have implicated AMPK in TGFβ signaling in other tissues (Lee et al., 2013; Lim et al., 2012), we demonstrate that AMPK provides post-transcriptional regulation of TGFβ-2, the most abundant TGFβ isoform produced by iPS-CMs. We suggest

that reduced TGFβ-2 is also a contributing mechanism for ventricular pre-excitation arrhythmias that patients with PRKAG2 mutations can have. The annulus fibrosus, a band of connective tissue that insulates and prevents direct electrophysiologic connections between the atria and ventricles, develops from the embryonic cardiac cushions in response to TGFβ-2 signals (Azhar et al., 2009). Consistent with this TGFβ-2 dependence, the annulus fibrosus is hypomorphic in PRKAG2 cardiomyopathy mouse models (Arad et al., 2003) and exhibits ventricular pre-excitation and arrhythmias. By activating AMPK and reducing TGFβ-2 production, we propose that PRKAG2 mutations that are selectively expressed in the heart may cause these developmental abnormalities.

Finally, we show that the potential for harnessing AMPK-dependent changes in TGFβ signaling. We demonstrate that A769662 prevented fibrosis and cardiac hypertrophy in HCM mice. Consistent with these observations, others have reported that AMPK inhibition exacerbates cardiac remodeling and dysfunction after thoracic-aortic banding (Shimano et al., 2010), while exercise promotes a reduction in cardiac fibrosis through AMPK-dependent mechanisms (Ma et al., 2015). AMPK activation also increased expression of PGC-1α and PPARα, potentially providing an improved metabolic profile to HCM hearts. We suggest that pulsatile AMPK activation by direct agonists, such as A769662, has the potential to reduce myocardial fibrosis that accompanies adverse remodeling and promotes arrhythmias in HCM and other cardiomyopathies.

In conclusion, the critical linkages between metabolism and transcript regulation that we report provide novel insights into AMPK signaling and the pathophysiologic mechanisms for PRKAG2 cardiomyopathy. The global transcriptional remodeling of metabolism that favors glycogen accumulation instead of glycolysis and crosstalk between AMPK activity and TGFβ signaling point to the complex roles by which altered AMPK activity impacts cardiac function. Small molecules that target AMPK activation are under development for several conditions, albeit with concerns that these may incite cardiomyopathy, similar to PRKAG2 mutations (Zaha and Young, 2012). Our findings indicate the considerable potential for molecules that provide tailored and intermittent AMPK activation to attenuate fibrosis and adverse remodeling in cardiomyopathies and many other forms of heart disease.

EXPERIMENTAL PROCEDURES

IPSC Production, Differentiation, and PRKAG2 Lentivirus

Patient samples were obtained after informed written consent using protocols approved by the Institutional Review Board of Partners HealthCare. Patient-specific iPSCs were produced from T cells (Loh et al., 2009) using STEMCCA lentivirus. IPSCs were screened for pluripotency markers (Figures S1F–S1H), copy number variants, karyotyping (Figure S1G), or virtual karyotyping using Illumina HumanOmniExpress-12 v1 arrays. iPSCs were maintained in feeder-free conditions and were differentiated to the CM lineage by small molecules (Lian et al., 2013). IPS-CMs were purified using metabolic selection (Tohyama et al., 2013) and studied on day 30–40 after initiation of differentiation. Following differentiation, iPS-CM purity was determined by fluorescence-activated cell sorting (FACS) analysis (>90% TnnT+) or by morphology. We amplified human PRKAG2 from a human iPS-CM cDNA library and inserted N488I and R531Q by site-directed mutagenesis (Agilent). We inserted sequence-verified PRKAG2 into the third generation lentivirus backbone pLenti (Addgene) and transduced iPS-CMs with MOI of 2.

TALEN Genome Editing

TALE nucleases were designed to flank the targeted mutation at N488I in human *PRKAG2* (Figure S1A) as previously described (Ding et al., 2013). Briefly, TALEN genomic binding sites 15 bp in length (Table S1A) were chosen within 30 bp of the nucleotide change required during homologous recombination. The TALEN pair, along with a correction, 50-mer ssODN (Table S1A) that encoded the wild-type *PRKAG2* sequence, were electroporated into $P_A^{N488I/WT}$ iPSCs. GFP/RFP double-positive iPSCs were sorted (Figure S1C), expanded, and Sanger sequenced (Tables S1B and S2) to confirm either scarless correction to wild-type ($P_{AT}^{N488I/WT}$) or in/dels that created a homozygous loss-of-function line ($P_{AT}^{KO/KO}$). Genotypes were validated with RFLP analysis using restriction enzyme digest with MSE1 (NEB) (Figures S1D and S1E). Experimental overview summarized in Figure S1B.

RNA-Sequencing and Computational Methods

Total RNA was isolated from day 30–40 iPS-CMs or 3-week-old mouse left ventricular tissue using TRIzol (Invitrogen). CDNA libraries were constructed using SuperScript III First-Strand Synthesis (Invitrogen). To reduce biologic variation among samples, cDNAs were pooled from at least biological triplicates for each sample and cDNA libraries were constructed using Nextera XT DNA Sample Preparation Kit (Illumina). Libraries were prepared and sequenced as described previously (Christodoulou et al., 2011) and were aligned with STAR (Engström et al., 2013). Differentially regulated transcripts were analyzed, and transcript network analysis was generated through the use of IPA (QIAGEN). For hierarchical cluster analysis, we used Cluster 3.0.

Cardiac Microtissues and Microcontact Printing

CMTs were prepared as previously described (Boudou et al., 2012). Micropatterned substrates were prepared as previously described (Tan et al., 2004).

Cell Size and Flow Cytometry Assays

Cell size was measured by determining cell area on micropatterned surface using ImageJ (NIH). IPS-CMs were disassociated and analyzed by flow cytometry using a LSRFortessa analyzer (BD). Cell size was determined by analyzing forward scatter (FSC). Mitochondrial content was measured by staining iPS-CMs with MitoTracker Green FM (Invitrogen) and analyzed using flow cytometry according to manufacturer's protocol. All FACS assays were done with at least biological triplicates.

LC-MS/MS Metabolomics and Other Metabolic Assays

Intracellular metabolites were extracted from day 30–40 iPS-CMs differentiated from TALEN isogenic iPSCs. All assays were done in biological triplicates. We performed metabolomic profiling using LC-MS/MS. For extended methods, see Supplemental Experimental Procedures. Seahorse XF24 (Seahorse Bioscience) was utilized to measure mitochondrial oxygen consumption according to manufacturers protocol. Glucose uptake was measured by biochemical methods from conditioned media using the glucose oxidase assay (Sigma), while lactate production was measured using a lactate dehydrogenase assay (Cayman). All metabolic assays were done with at least biological triplicates.

iPS-CM Viability and Cytotoxicity Assays

Day 30–40 iPS-CMs were cultured in two dimensional tissue culture formats and were stained for viability with ApoTox-Glo Assay (Promega). For doxorubicin (Tocris) experiments, iPS-CMs were exposed to doxorubicin (6 μM) for 12 hr prior to viability assay. For CMT viability experiments, propidium iodide (Invitrogen) was used according to manufacturer's protocol. PI+ nuclei were counted manually using ImageJ (NIH).

Western Blotting, Tissue Staining, and ELISA

IPS-CM lysates were solubilized in RIPA buffer followed by western blotting using Cell Signaling antibodies: AMPKα Duet, ACC Duet, AKT Duet, SMAD2 Duet, cardiac actinin A (Abcam), TGFβ, and GAPDH. ImageJ (NIH) was used to quantify western blot densitometries with at least three lanes per condition.

For imaging CMTs, we fixed CMTs with 4% PFA followed by staining with cardiac actinin A and DAPI. To measure conditioned media TGF-beta isoform production, we used Quantikine ELISA (R&D).

Mouse Protocols, Cardiac Imaging, and Fibrosis Quantification

All mice were maintained and studied using protocols approved by the Animal Care and Use Committee of Harvard Medical School. Studies used male heterozygous HCM ($MHC^{R403Q/+}$) mice that were in 129SvEv background and transgenic N488I that were in the FVB background. 6-week-old pre-hypertrophic HCM mice (n = 15 mice in each arm) were treated with either DMSO or A769662 (Cayman) subcutaneously once daily for 3 weeks at a dose of 30 mg/kg (Cool et al., 2006). To accelerate hypertrophy, mice were treated with 1 mg/g Cyclosporine A (CsA; Novartis), which was administered via oral chow. We studied male mice that more consistently develop HCM than do female littermates. Fibrosis was quantified using analysis of Masson trichrome stained sections. Cardiac hypertrophy was measured using a Vevo 770 Micro-Imager (VisualSonics). For extended methods, see Supplemental Experimental Procedures.

SUPPLEMENTAL INFORMATION

Supplemental Information includes Supplemental Experimental Procedures, five figures, seven tables, and two movies and can be found with this article online at http://dx.doi.org/10.1016/j.celrep.2016.11.066.

AUTHOR CONTRIBUTIONS

Conceptualization, J.T.H. and C.E.S.; Methodology, J.T.H., A.C., A.L., K.Z., R.M.G., R.K., J.O., G.R., J.G., K.M., R.E.G., S.M.W., C.S.C., J.G.S., and C.E.S.; Investigation, J.T.H., A.C., M.A.B., K.Z., C.C.S., A.L., H.W., and J.O.; Writing-Original Draft, J.T.H.; Writing-Review & Editing, all authors; and Funding Acquisition, J.T.H., C.S.C., J.G.S., and C.E.S. M.A.B. contributed RNA samples from pre-hypertrophic mouse models and assisted with computational analysis.

ACKNOWLEDGMENTS

We thank Barbara McDonough, Kaoru Ito, and Gregory Fishbein for their contributions. C.S.C. is the scientific founder of Innolign Biological, which is developing CMTs for commercial applications. This work was supported in part by grants from NIH HL125807 (to J.T.H.), AR062128 (to G.R.), UH3EB017103 (to C.S.C.), EB001046 (to C.S.C.), HL080494 (to J.G.S. and C.S.C.), HL128810 (to R.M.G.), HL084553 (to J.G.S.), John S. Ladue Foundation (to J.T.H.), Leducq Foundation (to J.G.S. and C.E.S.), Sarnoff Foundation (to C.C.S.), and the Howard Hughes Medical Institute (to C.E.S.).

Received: July 1, 2016
Revised: September 19, 2016
Accepted: November 21, 2016
Published: December 20, 2016; corrected online: May 25, 2017

REFERENCES

Arad, M., Benson, D.W., Perez-Atayde, A.R., McKenna, W.J., Sparks, E.A., Kanter, R.J., McGarry, K., Seidman, J.G., and Seidman, C.E. (2002). Constitutively active AMP kinase mutations cause glycogen storage disease mimicking hypertrophic cardiomyopathy. J. Clin. Invest. *109*, 357–362.

Arad, M., Moskowitz, I.P., Patel, V.V., Ahmad, F., Perez-Atayde, A.R., Sawyer, D.B., Walter, M., Li, G.H., Burgon, P.G., Maguire, C.T., et al. (2003). Transgenic mice overexpressing mutant PRKAG2 define the cause of Wolff-Parkinson-White syndrome in glycogen storage cardiomyopathy. Circulation *107*, 2850–2856.

Azhar, M., Runyan, R.B., Gard, C., Sanford, L.P., Miller, M.L., Andringa, A., Pawlowski, S., Rajan, S., and Doetschman, T. (2009). Ligand-specific function of transforming growth factor beta in epithelial-mesenchymal transition in heart development. Dev. Dyn. *238*, 431–442.

Baskin, K.K., and Taegtmeyer, H. (2011). AMP-activated protein kinase regulates E3 ligases in rodent heart. Circ. Res. *109*, 1153–1161.

Boudou, T., Legant, W.R., Mu, A., Borochin, M.A., Thavandiran, N., Radisic, M., Zandstra, P.W., Epstein, J.A., Margulies, K.B., and Chen, C.S. (2012). A microfabricated platform to measure and manipulate the mechanics of engineered cardiac microtissues. Tissue Eng. Part A *18*, 910–919.

Bultot, L., Guigas, B., Von Wilamowitz-Moellendorff, A., Maisin, L., Vertommen, D., Hussain, N., Beullens, M., Guinovart, J.J., Foretz, M., Viollet, B., et al. (2012). AMP-activated protein kinase phosphorylates and inactivates liver glycogen synthase. Biochem. J. *443*, 193–203.

Burwinkel, B., Scott, J.W., Bührer, C., van Landeghem, F.K., Cox, G.F., Wilson, C.J., Grahame Hardie, D., and Kilimann, M.W. (2005). Fatal congenital heart glycogenosis caused by a recurrent activating R531Q mutation in the gamma 2-subunit of AMP-activated protein kinase (PRKAG2), not by phosphorylase kinase deficiency. Am. J. Hum. Genet. *76*, 1034–1049.

Cai, B., Li, J., Wang, J., Luo, X., Ai, J., Liu, Y., Wang, N., Liang, H., Zhang, M., Chen, N., et al. (2012). microRNA-124 regulates cardiomyocyte differentiation of bone marrow-derived mesenchymal stem cells via targeting STAT3 signaling. Stem Cells *30*, 1746–1755.

Carney, D.H., Mann, R., Redin, W.R., Pernia, S.D., Berry, D., Heggers, J.P., Hayward, P.G., Robson, M.C., Christie, J., Annable, C., et al. (1992). Enhancement of incisional wound healing and neovascularization in normal rats by thrombin and synthetic thrombin receptor-activating peptides. J. Clin. Invest. *89*, 1469–1477.

Christodoulou, D.C., Gorham, J.M., Herman, D.S., and Seidman, J.G. (2011). Construction of normalized RNA-seq libraries for next-generation sequencing using the crab duplex-specific nuclease. Curr. Protoc. Mol. Biol. http://dx.doi.org/10.1002/0471142727.mb0412s94

Cool, B., Zinker, B., Chiou, W., Kifle, L., Cao, N., Perham, M., Dickinson, R., Adler, A., Gagne, G., Iyengar, R., et al. (2006). Identification and characterization of a small molecule AMPK activator that treats key components of type 2 diabetes and the metabolic syndrome. Cell Metab. *3*, 403–416.

Debold, E.P., Schmitt, J.P., Patlak, J.B., Beck, S.E., Moore, J.R., Seidman, J.G., Seidman, C., and Warshaw, D.M. (2007). Hypertrophic and dilated cardiomyopathy mutations differentially affect the molecular force generation of mouse alpha-cardiac myosin in the laser trap assay. Am. J. Physiol. Heart Circ. Physiol. *293*, H284–H291.

Ding, Q., Lee, Y.K., Schaefer, E.A., Peters, D.T., Veres, A., Kim, K., Kuperwasser, N., Motola, D.L., Meissner, T.B., Hendriks, W.T., et al. (2013). A TALEN genome-editing system for generating human stem cell-based disease models. Cell Stem Cell *12*, 238–251.

Doenst, T., Nguyen, T.D., and Abel, E.D. (2013). Cardiac metabolism in heart failure: implications beyond ATP production. Circ. Res. *113*, 709–724.

Engström, P.G., Steijger, T., Sipos, B., Grant, G.R., Kahles, A., Rätsch, G., Goldman, N., Hubbard, T.J., Harrow, J., Guigó, R., and Bertone, P.; RGASP Consortium (2013). Systematic evaluation of spliced alignment programs for RNA-seq data. Nat. Methods *10*, 1185–1191.

Geisterfer-Lowrance, A.A., Christe, M., Conner, D.A., Ingwall, J.S., Schoen, F.J., Seidman, C.E., and Seidman, J.G. (1996). A mouse model of familial hypertrophic cardiomyopathy. Science *272*, 731–734.

Gollob, M.H., Green, M.S., Tang, A.S., Gollob, T., Karibe, A., Ali Hassan, A.S., Ahmad, F., Lozado, R., Shah, G., Fananapazir, L., et al. (2001). Identification of a gene responsible for familial Wolff-Parkinson-White syndrome. N. Engl. J. Med. *344*, 1823–1831.

Hardie, D.G., Ross, F.A., and Hawley, S.A. (2012). AMPK: a nutrient and energy sensor that maintains energy homeostasis. Nat. Rev. Mol. Cell Biol. *13*, 251–262.

Hinson, J.T., Chopra, A., Nafissi, N., Polacheck, W.J., Benson, C.C., Swist, S., Gorham, J., Yang, L., Schafer, S., Sheng, C.C., et al. (2015). HEART DISEASE. Titin mutations in iPS cells define sarcomere insufficiency as a cause of dilated cardiomyopathy. Science *349*, 982–986.

Ho, C.Y., López, B., Coelho-Filho, O.R., Lakdawala, N.K., Cirino, A.L., Jarolim, P., Kwong, R., González, A., Colan, S.D., Seidman, J.G., et al. (2010).

Myocardial fibrosis as an early manifestation of hypertrophic cardiomyopathy. N. Engl. J. Med. *363*, 552–563.

Ikeda, S., He, A., Kong, S.W., Lu, J., Bejar, R., Bodyak, N., Lee, K.H., Ma, Q., Kang, P.M., Golub, T.R., and Pu, W.T. (2009). MicroRNA-1 negatively regulates expression of the hypertrophy-associated calmodulin and Mef2a genes. Mol. Cell. Biol. *29*, 2193–2204.

Kim, M., Hunter, R.W., Garcia-Menendez, L., Gong, G., Yang, Y.Y., Kolwicz, S.C., Jr., Xu, J., Sakamoto, K., Wang, W., and Tian, R. (2014). Mutation in the γ2-subunit of AMP-activated protein kinase stimulates cardiomyocyte proliferation and hypertrophy independent of glycogen storage. Circ. Res. *114*, 966–975.

Kraegen, E.W., Sowden, J.A., Halstead, M.B., Clark, P.W., Rodnick, K.J., Chisholm, D.J., and James, D.E. (1993). Glucose transporters and in vivo glucose uptake in skeletal and cardiac muscle: fasting, insulin stimulation and immunoisolation studies of GLUT1 and GLUT4. Biochem. J. *295*, 287–293.

Kurth-Kraczek, E.J., Hirshman, M.F., Goodyear, L.J., and Winder, W.W. (1999). 5′ AMP-activated protein kinase activation causes GLUT4 translocation in skeletal muscle. Diabetes *48*, 1667–1671.

Lang, T., Yu, L., Tu, Q., Jiang, J., Chen, Z., Xin, Y., Liu, G., and Zhao, S. (2000). Molecular cloning, genomic organization, and mapping of PRKAG2, a heart abundant gamma2 subunit of 5′-AMP-activated protein kinase, to human chromosome 7q36. Genomics *70*, 258–263.

Lee, J.H., Kim, J.H., Kim, J.S., Chang, J.W., Kim, S.B., Park, J.S., and Lee, S.K. (2013). AMP-activated protein kinase inhibits TGF-β-, angiotensin II-, aldosterone-, high glucose-, and albumin-induced epithelial-mesenchymal transition. Am. J. Physiol. Renal Physiol. *304*, F686–F697.

Lehmann, J.M., Moore, L.B., Smith-Oliver, T.A., Wilkison, W.O., Willson, T.M., and Kliewer, S.A. (1995). An antidiabetic thiazolidinedione is a high affinity ligand for peroxisome proliferator-activated receptor gamma (PPAR gamma). J. Biol. Chem. *270*, 12953–12956.

Li, J., Ren, J., Liu, X., Jiang, L., He, W., Yuan, W., Yang, J., and Dai, C. (2015). Rictor/mTORC2 signaling mediates TGFβ1-induced fibroblast activation and kidney fibrosis. Kidney Int. *88*, 515–527.

Lian, X., Zhang, J., Azarin, S.M., Zhu, K., Hazeltine, L.B., Bao, X., Hsiao, C., Kamp, T.J., and Palecek, S.P. (2013). Directed cardiomyocyte differentiation from human pluripotent stem cells by modulating Wnt/β-catenin signaling under fully defined conditions. Nat. Protoc. *8*, 162–175.

Lim, J.Y., Oh, M.A., Kim, W.H., Sohn, H.Y., and Park, S.I. (2012). AMP-activated protein kinase inhibits TGF-β-induced fibrogenic responses of hepatic stellate cells by targeting transcriptional coactivator p300. J. Cell. Physiol. *227*, 1081–1089.

Loh, Y.H., Agarwal, S., Park, I.H., Urbach, A., Huo, H., Heffner, G.C., Kim, K., Miller, J.D., Ng, K., and Daley, G.Q. (2009). Generation of induced pluripotent stem cells from human blood. Blood *113*, 5476–5479.

Lovekamp-Swan, T., Jetten, A.M., and Davis, B.J. (2003). Dual activation of PPARalpha and PPARgamma by mono-(2-ethylhexyl) phthalate in rat ovarian granulosa cells. Mol. Cell. Endocrinol. *201*, 133–141.

Ma, X., Fu, Y., Xiao, H., Song, Y., Chen, R., Shen, J., An, X., Shen, Q., Li, Z., and Zhang, Y. (2015). Cardiac fibrosis alleviated by exercise training is AMPK-dependent. PLoS ONE *10*, e0129971.

Marsin, A.S., Bertrand, L., Rider, M.H., Deprez, J., Beauloye, C., Vincent, M.F., Van den Berghe, G., Carling, D., and Hue, L. (2000). Phosphorylation and activation of heart PFK-2 by AMPK has a role in the stimulation of glycolysis during ischaemia. Curr. Biol. *10*, 1247–1255.

McGee, S.L., van Denderen, B.J., Howlett, K.F., Mollica, J., Schertzer, J.D., Kemp, B.E., and Hargreaves, M. (2008). AMP-activated protein kinase regulates GLUT4 transcription by phosphorylating histone deacetylase 5. Diabetes *57*, 860–867.

Murphy, R.T., Mogensen, J., McGarry, K., Bahl, A., Evans, A., Osman, E., Syrris, P., Gorman, G., Farrell, M., Holton, J.L., et al. (2005). Adenosine monophosphate-activated protein kinase disease mimicks hypertrophic cardiomyopathy and Wolff-Parkinson-White syndrome: natural history. J. Am. Coll. Cardiol. *45*, 922–930.

Ofir, M., Arad, M., Porat, E., Freimark, D., Chepurko, Y., Vidne, B.A., Seidman, C.E., Seidman, J.G., Kemp, B.E., and Hochhauser, E. (2008). Increased glycogen stores due to gamma-AMPK overexpression protects against ischemia and reperfusion damage. Biochem. Pharmacol. *75*, 1482–1491.

Pöyhönen, P., Hiippala, A., Ollila, L., Kaasalainen, T., Hänninen, H., Heliö, T., Tallila, J., Vasilescu, C., Kivistö, S., Ojala, T., and Holmström, M. (2015). Cardiovascular magnetic resonance findings in patients with PRKAG2 gene mutations. J. Cardiovasc. Magn. Reson. *17*, 89.

Reznick, R.M., Zong, H., Li, J., Morino, K., Moore, I.K., Yu, H.J., Liu, Z.X., Dong, J., Mustard, K.J., Hawley, S.A., et al. (2007). Aging-associated reductions in AMP-activated protein kinase activity and mitochondrial biogenesis. Cell Metab. *5*, 151–156.

Rupérez, M., Lorenzo, O., Blanco-Colio, L.M., Esteban, V., Egido, J., and Ruiz-Ortega, M. (2003). Connective tissue growth factor is a mediator of angiotensin II-induced fibrosis. Circulation *108*, 1499–1505.

Scott, J.W., Hawley, S.A., Green, K.A., Anis, M., Stewart, G., Scullion, G.A., Norman, D.G., and Hardie, D.G. (2004). CBS domains form energy-sensing modules whose binding of adenosine ligands is disrupted by disease mutations. J. Clin. Invest. *113*, 274–284.

Shimano, M., Ouchi, N., Shibata, R., Ohashi, K., Pimentel, D.R., Murohara, T., and Walsh, K. (2010). Adiponectin deficiency exacerbates cardiac dysfunction following pressure overload through disruption of an AMPK-dependent angiogenic response. J. Mol. Cell. Cardiol. *49*, 210–220.

Sidhu, J.S., Rajawat, Y.S., Rami, T.G., Gollob, M.H., Wang, Z., Yuan, R., Marian, A.J., DeMayo, F.J., Weilbacher, D., Taffet, G.E., et al. (2005). Transgenic mouse model of ventricular preexcitation and atrioventricular reentrant tachycardia induced by an AMP-activated protein kinase loss-of-function mutation responsible for Wolff-Parkinson-White syndrome. Circulation *111*, 21–29.

Tan, J.L., Liu, W., Nelson, C.M., Raghavan, S., and Chen, C.S. (2004). Simple approach to micropattern cells on common culture substrates by tuning substrate wettability. Tissue Eng. *10*, 865–872.

Teekakirikul, P., Eminaga, S., Toka, O., Alcalai, R., Wang, L., Wakimoto, H., Nayor, M., Konno, T., Gorham, J.M., Wolf, C.M., et al. (2010). Cardiac fibrosis in mice with hypertrophic cardiomyopathy is mediated by non-myocyte proliferation and requires Tgf-β. J. Clin. Invest. *120*, 3520–3529.

Tian, R., Musi, N., D'Agostino, J., Hirshman, M.F., and Goodyear, L.J. (2001). Increased adenosine monophosphate-activated protein kinase activity in rat hearts with pressure-overload hypertrophy. Circulation *104*, 1664–1669.

Tohyama, S., Hattori, F., Sano, M., Hishiki, T., Nagahata, Y., Matsuura, T., Hashimoto, H., Suzuki, T., Yamashita, H., Satoh, Y., et al. (2013). Distinct metabolic flow enables large-scale purification of mouse and human pluripotent stem cell-derived cardiomyocytes. Cell Stem Cell *12*, 127–137.

Widyantoro, B., Emoto, N., Nakayama, K., Anggrahini, D.W., Adiarto, S., Iwasa, N., Yagi, K., Miyagawa, K., Rikitake, Y., Suzuki, T., et al. (2010). Endothelial cell-derived endothelin-1 promotes cardiac fibrosis in diabetic hearts through stimulation of endothelial-to-mesenchymal transition. Circulation *121*, 2407–2418.

Zaha, V.G., and Young, L.H. (2012). AMP-activated protein kinase regulation and biological actions in the heart. Circ. Res. *111*, 800–814.